*energies*

MDPI

*Article*

# Palladium-Functionalized Graphene for Hydrogen Sensing Performance: Theoretical Studies

**Vinay Kishnani [1,†], Anshul Yadav [2,†], Kunal Mondal [3,4,*] and Ankur Gupta [1,*]**

[1] Department of Mechanical Engineering, Indian Institute of Technology, Jodhpur 342037, Rajasthan, India; kishnani.1@iitj.ac.in
[2] Membrane Science and Separation Technology, CSIR Central Salt and Marine Chemicals Research Institute, Bhavnagar 364002, Gujarat, India; anshuly@csmcri.res.in
[3] Materials Science and Engineering Department, Idaho National Laboratory, Idaho Falls, ID 83415, USA
[4] Department of Civil & Environmental Engineering, Idaho State University, Pocatello, ID 83209, USA
* Correspondence: Kunal.Mondal@inl.gov (K.M.); ankurgupta@iitj.ac.in (A.G.)
† Equal Contribution.

**Abstract:** The adsorption characteristics of $H_2$ molecules on the surface of Pd-doped and Pd-decorated graphene (G) have been investigated using density functional theory (DFT) calculations to explore the sensing capabilities of Pd-doped/decorated graphene. In this analysis, electrostatic potential, atomic charge distribution, 2D and 3D electron density contouring, and electron localization function projection, were investigated. Studies have demonstrated the sensing potential of both Pd-doped and Pd-decorated graphene to $H_2$ molecules and have found that the gap between the highest occupied molecular orbital (HOMO) and the lowest unoccupied molecular orbital (LUMO), i.e., the HOMO-LUMO gap (HLG), decreases to 0.488 eV and 0.477eV for Pd-doped and Pd-decorated graphene, respectively. When $H_2$ is adsorbed on these structures, electrical conductivity increases for both conditions. Furthermore, chemical activity and electrical conductivity are higher for Pd-decorated G than Pd-doped G, whereas the charge transfer of Pd-doped graphene is far better than that of Pd-decorated graphene. Also, studies have shown that the adsorption energy of Pd-doped graphene (−4.3 eV) is lower than that of Pd-decorated graphene (−0.44 eV); a finding attributable to the fact that the recovery time for Pd-decorated graphene is lower compared to Pd-doped graphene. Therefore, the present analysis confirms that Pd-decorated graphene has a better $H_2$ gas sensing platform than Pd-doped graphene and, as such, may assist the development of nanosensors in the future.

**Keywords:** density functional theory; hydrogen sensing; palladium



**Citation:** Kishnani, V.; Yadav, A.; Mondal, K.; Gupta, A. Palladium-Functionalized Graphene for Hydrogen Sensing Performance: Theoretical Studies. *Energies* **2021**, *14*, 5738. https://doi.org/10.3390/en14185738

Academic Editor: Vladislav A. Sadykov

Received: 18 August 2021
Accepted: 8 September 2021
Published: 12 September 2021



## 1. Introduction

Understanding the various kinds of interactions between metallic molecules and graphene is of utmost importance if a number of scientific problems, associated with the enhancement of sensing performance, are to be solved. Over the last few decades, semiconducting materials such as hydrogen sensing films have been extensively explored [1,2]. Carbon-based nanomaterials and their derivatives, viz., graphene, reduced graphene, reduced graphene oxide, carbon nanotubes, and fullerene, play a vital role in gas sensing, adsorption, and storage performance due to their interesting and beneficial chemical and physical properties [3–6]. Carbon-based nanomaterials possess the largest mechanical strength, high specific surface area, good conductivity, compatibility with surface modification, and high electron mobility [7–10]. As such, they have found widespread applications in the fields of electronics, chemistry, and medicine; as catalysts in gas sensors; and as components in the pursuit of energy conversion, production, and storage [11–19]. Graphene and its oxide derivatives have numerous properties to choose from and, for this reason, are an ideal gas sensor material. Some of these properties include: (1) large

surface area, which provides better interaction with gas molecules; (2) charge transfer capabilities; and (3) hybridization, which results in strong interaction between the electronic state of graphene and gas molecules [20,21]. Despite these advantages, the lack of bandgap in graphene limits its use in electronic devices. Graphene nanoflakes and graphene nanoribbons are $H_2$-passivated, graphene-based, materials of finite width [22]. Over recent decades, many transition materials have been explored to enhance sensing capabilities, adsorbance, and storage properties. Additionally, the ability of graphene and its oxides to sense various gases has been investigated. Previously, researchers used transition metals to decorate graphene, thus enhancing its surface reactivity and facilitating the separation of targeted gases. Cu [23], Au [24], Pd [25], Fe [26], Ru [27], and Mn [28] are only some of the transition metals frequently reported on in the literature. The reason we selected Pd in this work was because of Pd's greater affinity towards hydrogen gas [29–31]. Alfano et al. [32] developed a fully eco-friendly, Pd-decorated, graphene device for fast and selective detection of $H_2$ within a 30 s timeframe and with a 26% response value for exposure of 1% $H_2$. Singla et al. [33] studied the hydrogen sensing mechanism of a copper-decorated, N-doped, defective graphene through DFT calculation and found that it increased the binding energy of Cu atoms due to the deficiency of electrons in the N-doped site preventing the aggregation of the metal in their graphene sheets. It was also found that hydrogen adsorption intensity was much higher for the copper-decorated complex system. In other work, Bakshi et al. [34] studied the hydrogen storage capabilities of these new adsorbents by introducing Pd into co-doped, pristine and defective, graphene sheets containing $N_2$ and boron as adatoms. They reported that Pd enhanced the hydrogen adsorption energy of the pristine graphene, whereas the defective sheets prevented clustering, resulting in a reduction to hydrogen adsorption. Thus, hydrogen adsorption can be enhanced by doping graphene sheets with $N_2$ and boron adatoms. Finally, results concluded that Pd-decorated, N-B co-doped, graphene sheets behave as a novel material for hydrogen adsorption. Zhou et al. [35] studied the adsorption of TCDF on vacancy-defective graphene doped with Mn and Fe via DFT calculations and reported enhanced sensitivity of the graphene towards the TCDF molecule due to the presence of vacancy and dopants. From this investigation, Zhou et al. found that the hydrogen adsorption of $Ni_4$ clusters embedded in multi-vacancy defective graphene absorbed up to four hydrogen molecules in circumstances conducive to hydrogen storage [36]. In another study, the hydrogen storage of a graphene-Pd(T) graphene sandwich structure was studied, with findings suggesting that the binding energy of the Pd atoms at the T-sites of the bilayer graphene is higher than the experimental cohesion energy of the Pd atoms; this resulted in the elimination of a metal cluster effect on the adsorption property, producing an outstanding $H_2$ storage material [37]. Gecim et al.'s [38] work focused on the methanol sensing capabilities of Ga- and Ge-doped graphene using DFT calculations and found that, during adsorption, Ga- and Ge-doped graphene increased the positive charge of methanol transfer to graphene as well as electrical conductivity. At the same time, the gap between HOMO and LUMO decreases for the doped transition metals. It was also observed that Ge-doped graphene had higher electrical conductivity, a shorter recovery time, and increased sensitivity for methanol compared to Ga-doped graphene. Zheng et al. [39] studied the hydrogen storage performance of pure graphene nanoribbon and Li-decorated graphene using a DFT calculation study. The results revealed that the Li atom contains high interaction energy towards pure graphene ribbon with a high adsorption energy, and has little effect on geometry. At the same time, $H_2$ molecules interact strongly with Li-decorated graphene, suggesting that Li-decorated graphene nanoribbon exhibits excellent hydrogen storage capability. Ostad et al. [40] investigated the adsorption of transition metal clusters over a graphene layer through DFT and identified the site between the two neighboring carbon atoms as the most stable for Pt, Pd, and Ir adatoms. These authors determined that, as the number of atoms increases, the binding energy of the cluster also increases. By contrast, the adsorption energy of the cluster attached to the graphene lowered when the lowest energy configuration for the graphene-transition metal was applied. The adsorption energy of the adatoms

increases due to the Van der Waals correction applied in the DFT calculation. The charge transmitted to the carbon atom via transition metal atoms was also investigated, showing that the d orbital of the adatoms introduced a peak at the dirac point of the graphene. In another study, Montejo-Alvaro et al. [41] investigated the properties and ground-state structure of the $Pd_n$ cluster (n = 3–10) using DFT calculation and found it was supported on pristine, B-doped, and defective graphene quantum dots. They also reported that reactivity towards oxygen reduction was partially improved. In another work, hydrogen adsorption on Ni (111) surfaces, $Ni_{13}$–graphene, and isolated $Ni_{13}$ clusters through DFT calculation, were studied. Through pseudo charge density difference calculation, a build-up of charge density in the region of the Ni-graphene interfacial was observed. An activation barrier that stabilizes $Ni_{13}$-graphene was observed using hydrogen adsorption [42]. Cui et al. [43] conducted a DFT calculation study to assess the sensing behavior of $SOF_2$ and $SO_2F_2$ molecules using the surface of Pt/Pd-decorated CNT and $Pt_2Pd_2$-decorated CNT. The study found that decorated CNT had better adsorption ability for $SOF_2$ compared to $SO_2F_2$, and that large charge transfer numbers were generated by enlarging the bandgap after adsorption and redistribution of the total electrons in the adsorption system due to the strong interaction between the surface and $SOF_2$ molecule. Cheng et al. [44] investigated the sensitivity enhancement of a Pd-decorated ZnO nanocluster for $H_2$ sensing via DFT calculation. They found that Pd released 42.1 kcal/mol energy and that it was located above the center of the tetragonal ring. Furthermore, adsorption of the $O_2$ molecule on the Pd atom weakened the O-O bond, resulting in a good site for $H_2$ attachment requiring 1.3 kcal/mol as an energy barrier at 325 K temperature. Response time also increased from 0.11 to 123.53 for the Pd-decorated ZnO nanocluster, and the prediction of recovery time was 0.7 ms for $H_2O$ desorption in the case of the Pd-decorated ZnO nanocluster. Khodadadi et al. [45] evaluated the sensing characteristics of $H_2S$ through doped and decorated metals attached to graphene and found that doping of transition metals (Ni, Cu, and Zn) enhanced the molecular adsorption of $H_2S$ among all tested metals. Cu showed the best adsorption system due to low adsorption energy and a short distance. While, for metal decoration, Ni showed the lowest distance between the metal and carbon atom best suited for electron transfer from $H_2S$ to metal-decorated graphene.

In this work, the sensing characteristics of $H_2$ on both Pd-doped and Pd-decorated graphene were investigated using DFT calculations to analyze the effect of Pd-doping and Pd-decoration upon graphene sensitivity towards these molecules.

## 2. Computational Method

The adsorption process of the $H_2$ molecule on Pd-doped and Pd-decorated graphene was investigated via DFT calculations [46], using the Gaussian09 software [47]. The graphene structures were optimized by employing the B3PW9 method with a basis set of 6–31 g*. To plot the density of states (DOS) the GaussSum package was used [48] and the remaining 3D plots were plotted through Multiwfn. Adsorption energies and optimized geometry were based on Equilibrium Geometry calculations.

$$E = E_{electronic} + \text{Zero-point energy (ZPE)} + E_{vibrational} + E_{rotational} + E_{translational} \quad (1)$$

All energy values were calculated at room temperature (298 K) and atmospheric pressure, including zero-point energy and single-point energy. The Gaussian09 software was used to obtain the total thermal energy, vibrational frequency, enthalpy, and thermal free energy [49].

$$H = E + RT \quad (2)$$

where E stands for thermal energy, H for thermal enthalpy, R for ideal gas constant, and T for temperature (298 K).

The electronic properties of the $H_2$, adsorbed on the Pd-doped and Pd-decorated graphene, were investigated and compared. To evaluate the interaction between the $H_2$

molecule and the Pd-doped graphene, their adsorption energy ($E_{ads}$) was calculated with Equation (3).

$$\text{Adsorption Energy; } (\Delta E_{ads}) = E_{system} - (E_{cluster} + E_{adsorptive}) \quad (3)$$

where $E_{system}$ stands for the total energy of the $H_2$ on Pd-doped graphene geometry, $E_{cluster}$ stands for the energy of optimized Pd-doped graphene geometry, and $E_{adsorptive}$ stands for the energy of optimized $H_2$ geometry. To evaluate the interaction between the $H_2$ molecule and the Pd-decorated graphene, their adsorption energy ($E_{ads}$) was calculated with Equation (3), similar to the calculation for Pd-doped graphene.

$$\text{Adsorption Energy } (\Delta E_{ads}) = E_{system} - (E_{cluster} + E_{adsorptive})$$

where $E_{system}$ stands for the total energy of the $H_2$ on Pd-decorated graphene geometry, $E_{cluster}$ stands for the energy of optimized Pd-decorated graphene geometry, and $E_{adsorptive}$ stands for the energy of optimized $H_2$ geometry. As per the results, a negative value for the adsorption energy was obtained, indicating a stable structure and the occurrence of an exothermic process. The difference between the energy of HOMO and LUMO (HLG) was used to evaluate the chemical activity of Pd-doped and Pd-decorated graphene structures. Low HLG values imply that chemical activity is high for that atomic condition, and vice versa [50,51]. Furthermore, chemical hardness, electronegativity, electrophilicity, and chemical potential were calculated [52–54] to investigate the activity of the clusters. These values are based on Koopman's approach [55,56].

$$\text{Chemical Potential } (\mu) = -\frac{I + A}{2} \quad (4)$$

$$\text{Chemical Hardness } (\eta) = \frac{I - A}{2} \quad (5)$$

$$\text{Electrophilicity } (\omega) = \frac{\mu^2}{2\eta} \quad (6)$$

$$\text{Electronegativity } (\lambda) = -\mu \quad (7)$$

where $I = -\varepsilon$ HOMO and $A = -\varepsilon$ LUMO, $\varepsilon$HOMO-. To estimate net charge transfers and atomic charges; natural bond orbital charges, i.e., NBO population analysis, was applied [57]. The minimum electrophilicity principle [58] and maximum hardness principle [59] determined that the chemical stability of a system has a positive correlation with hardness and a negative correlation with electrophilicity.

## 3. Results and Discussion

A DFT optimized geometry of Pd-doped/decorated graphene before, and after, adsorption of $H_2$ molecules is shown in Figure 1.

In this process, a carbon atom of pristine graphene was substituted with a dopant atom (Pd) for the doped condition. The Pd atom was attached to the carbon atom by forming an external bond without affecting the electron density of the Pd-decorated graphene surface. This demonstrates that, after doping/decorating the Pd atom to the graphene, the intermolecular bond between the C-C atom increases in comparison to pristine graphene. The estimated lengths between the three carbon atoms and the Pd atom were 1.80 Å, 1.81 Å, and 1.82 Å for the doped condition (Figure 1a). For the decorated state, the length between the Pd atom and the carbon atom was 2.13 Å (Figure 1c). In addition, after adsorption of $H_2$ gas, the lengths between the three carbon atoms and Pd increased to 1.97 Å, 2.0 Å, and 2.0 Å for the doped condition, whereas molecular distance between the $H_2$ and Pd molecules measured up to 2.34 Å (Figure 1b). There was no change in the bond length of the carbon and Pd atoms for the decorated condition; however, the $H_2$ molecule attached to the Pd atom directly at a bond length of 1.85 Å (Figure 1d).

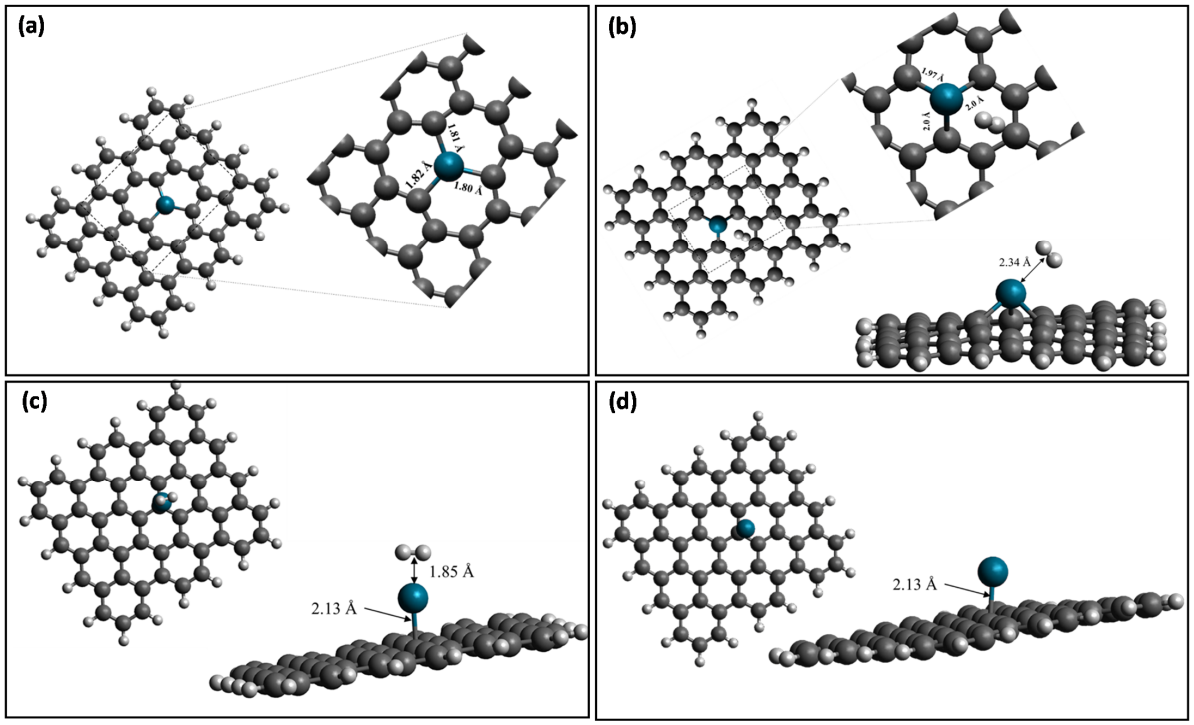


**Figure 1.** DFT optimized geometries of (**a**) Pd-doped graphene, (**b**) Pd-doped graphene-$H_2$, (**c**) Pd-decorated graphene, (**d**) Pd-decorated graphene-$H_2$.

The electrostatic potential behavior of Pd-doped and Pd-decorated graphene clusters before, and after, adsorption of $H_2$ is shown in Figure 2.

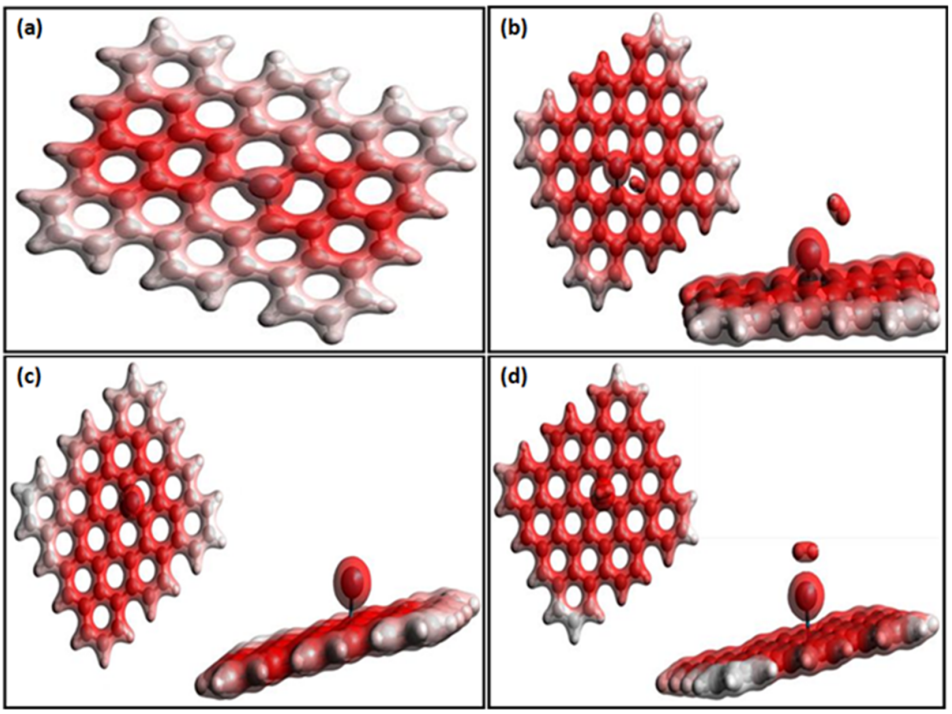


**Figure 2.** Electrostatic potential of (**a**) Pd-doped graphene, (**b**) Pd-doped graphene-$H_2$, (**c**) Pd-decorated graphene, (**d**) Pd-decorated graphene-$H_2$. The charge accumulation regions are in red.

It is clearly demonstrated that the charge accumulation in the doped region is less in comparison to Pd-decorated graphene, and that charge accumulation increases for both

conditions following adsorption of the $H_2$ molecules. The charge accumulation regions are depicted in red.

To determine the stability of configurations, the hydrogen molecule was located above the Pd-doped/decorated graphene cluster. To determine the characteristic behaviour of hydrogen adsorption over the Pd-doped/decorated graphene cluster, the calculation was computed for adsorption energies and adsorption enthalpies. This is shown in Tables 1 and 2.

**Table 1.** Properties of the Pd-doped graphene cluster before and after $H_2$ interaction.

| Properties | | Pd-Doped Graphene | $H_2$ Adsorbed on Pd-Doped Graphene |
|---|---|---|---|
| Distances (Å) | Pd-C | 1.80, 1.81,1.82Å | 1.97 Å, 2.0 Å, 2.0 Å |
| | Pd-H | | 2.34 Å |
| | H-H | 0.74 | 0.759 |
| NBO charges (e) | Pd atom | 1.214 | 1.006 |
| | C atoms (bonded with Pd) | −0.274, −0.274, −0.274 | −0.215, −0.174, −0.191 |
| | Adsorbed $H_2$ molecule | —- | 0, 0.067 |
| Adsorption energies (eV) | ΔE | —- | −4.3 |
| α MOs (eV) | HOMO | −4.171 | −3.999 |
| | LUMO | −3.611 | −3.511 |
| | HLG | 0.56 | 0.488 |
| | Chemical Hardness | 0.28 | 0.244 |
| | Chemical Potential | −3.891 | −3.755 |
| | Electronegativity | 3.891 | 3.755 |
| | Electrophilicity | 27.035 | 28.893 |

**Table 2.** Properties of the Pd-decorated graphene cluster before and after $H_2$ interaction.

| Properties | | Pd-Decorated Graphene | $H_2$ Adsorbed on Pd-Decorated Graphene |
|---|---|---|---|
| Distances (Å) | Pd-C | 2.13 | 2.13 |
| | Pd-H | – | 1.85 |
| | H-H | 0.74 | 0.803 |
| NBO charges (e) | Pd atom | 0.599 | 0.484 |
| | C atoms (bonded with Pd) | 0.006 | −0.073 |
| | Absorbed $H_2$ molecule | - | 0.023, 0.027 |
| Adsorption energies (eV) | ΔE | | −0.44 |
| α MOs (eV) | HOMO | −4.008 | −3.937 |
| | LUMO | −3.499 | −3.414 |
| | HLG | 0.509 | 0.477 |
| | Chemical Hardness | 0.254 | 0.238 |
| | Chemical Potential | −3.754 | −3.676 |
| | Electronegativity | 3.754 | 3.676 |
| | Electrophilicity | 27.741 | 28.388 |

The bond length between Pd-C atoms increases after the adsorption of $H_2$ molecules for both the Pd-doped/decorated graphene clusters. The new estimated bond lengths following $H_2$ adsorption were 1.97 Å, 2.0 Å, and 2.0 Å for the Pd-doped graphene clusters. No change in bond length between Pd-C for the Pd-decorated graphene occurred, as shown in Figure 1. The adsorption of hydrogen on both Pd-doped and Pd-decorated graphene structures is an exothermic process. Adsorption energies for the Pd-doped, and Pd-decorated, graphene clusters were calculated as −4.3 eV and −0.44 eV, respectively. The H-H bond length for the adsorbed hydrogen molecule was calculated as 0.759 Å for the Pd-doped graphene, and as 0.803 Å for the Pd-decorated graphene clusters. Both values were more significant than that of the free hydrogen molecule (0.74 Å).

To estimate the atomic charge and total charge transfer, the natural bond orbital population was applied [57], as shown in the Figure 3.

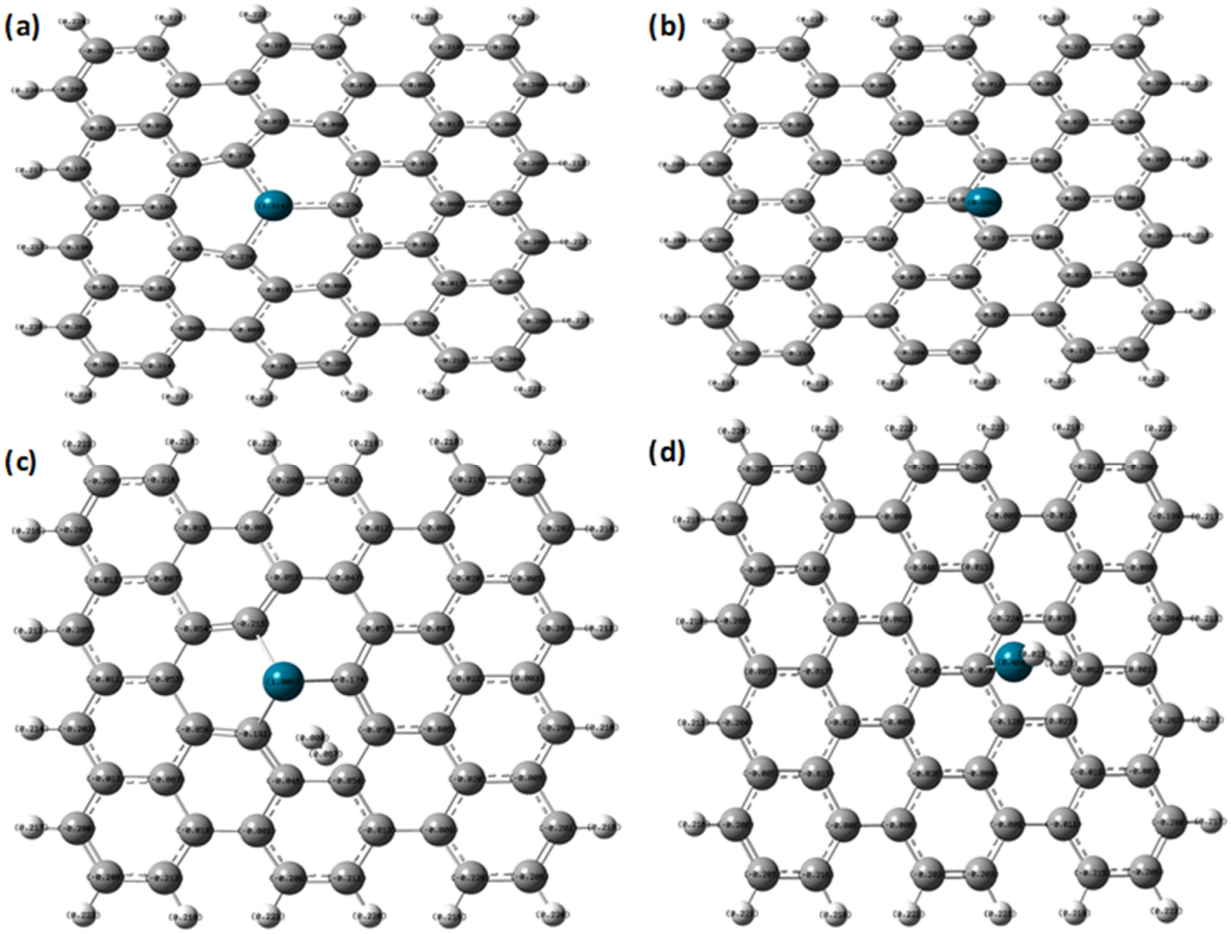


**Figure 3.** NBO atomic charge distributions for the optimised structures of (**a**) Pd-doped graphene, (**b**) Pd-decorated graphene, (**c**) Pd-doped graphene-$H_2$, and (**d**) Pd-decorated graphene-$H_2$.

While performing calculations for Pd-doped graphene and Pd-decorated graphene clusters, $H_2$ was adsorbed on both Pd-doped and Pd-decorated graphene clusters. The highest positive charges were observed for Pd atoms in both conditions (+1.214e for Pd-doped graphene and +0.599e for Pd-decorated graphene) and charges after $H_2$ adsorption (+1.006e for Pd-doped graphene and +0.484e for Pd-decorated graphene). To determine the electronic behavior of both clusters, the net charge transfers of adsorbed $H_2$ onto both Pd-doped graphene and Pd-decorated graphene clusters, were examined. Prior to adsorption, $H_2$ molecules had no charge; the net charge transferred to adsorbed $H_2$ molecules on Pd-doped and Pd-decorated graphene was calculated as (0, +0.067) and (+0.023, +0.027), respectively. The results suggest that the charge was transferred from $H_2$

to Pd-doped/decorated-graphene. With respect to the charge transfer comparisons, results suggest that the charge transferred from $H_2$ to Pd-doped graphene far quicker than to Pd-decorated graphene. This clearly demonstrates the difference in the adsorption energy for Pd-doped and Pd-decorated graphene clusters.

The molecular orbital (HOMO and LUMO) representation for both Pd-doped and Pd-decorated graphene is shown in Figure 4.

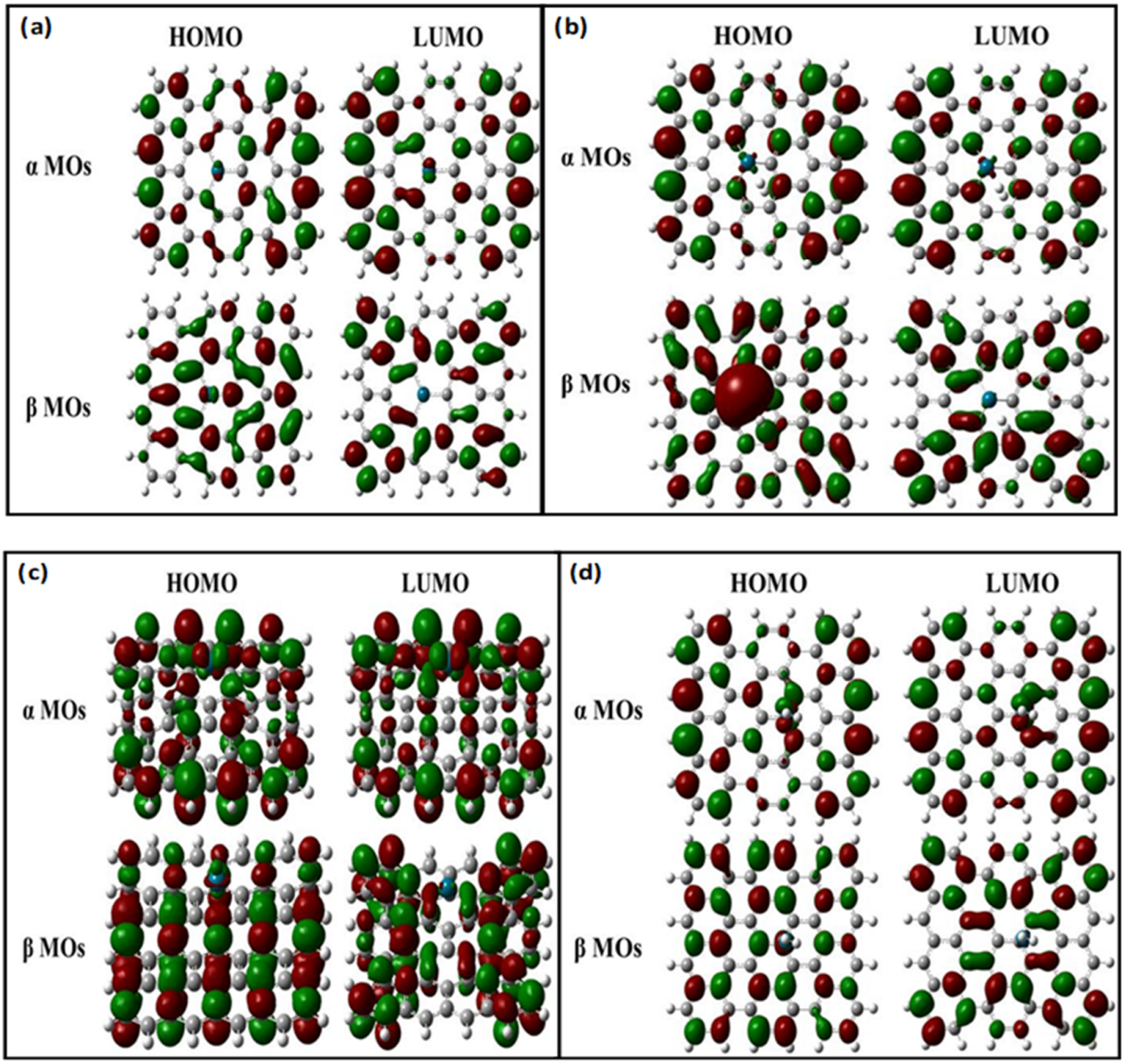


**Figure 4.** HOMO and LUMO representations of α and βMOs for the optimised structures of (**a**) Pd-doped graphene, (**b**) Pd-doped graphene-$H_2$, (**c**) Pd-decorated graphene, and (**d**) Pd-decorated graphene-$H_2$.

Figure 4a shows HOMO and LUMO representations of α and βMOs for the optimized structure of Pd-doped graphene. Figure 4c shows optimised structure representations for Pd-decorated graphene. The term α MOs is used for the spin-up, and βMOs for spin-down. The HLG is used to determine the chemical activity of Pd-doped and Pd-decorated graphene clusters HLG $\alpha \frac{1}{\text{Chemical Activity}}$; the lower the value of HLG, the higher the chemical activity [50,51]. The value of electrophilicity, electronegativity, HLG, HOMO, LUMO, chemical hardness, and chemical potential for Pd-doped and Pd-decorated graphene, is given in Tables 1 and 2. Adsorption energy is a dependent term for chemical potential; if

the chemical potential is low, then the adsorption energy for $H_2$ is also low [60,61]. HLG for Pd-doped graphene (0.56) is comparatively higher than Pd-decorated graphene (0.509), i.e., chemical activity of Pd-decorated graphene is higher than Pd-doped graphene. While, after the hydrogen adsorption, HLG for Pd-doped graphene decreased up to 0.488, meaning that chemical activity increased for Pd-decorated HLG value and decreases up to 0.477, the results demonstrate that chemical activity is higher for Pd-decorated graphene in comparison to Pd-doped graphene when all these conditions are met. For Pd-doped graphene, chemical hardness and electronegativity decreased following $H_2$ adsorption, whereas the amount of chemical potential and electrophilicity increased. For Pd-decorated graphene, chemical hardness and electronegativity decreases as the amount of chemical potential and electrophilicity increases. In comparison to Pd-doped and Pd-decorated graphene, the $H_2$ adsorption value of chemical hardness, electronegativity, and electrophilicity decreased as the value of chemical potential increased.

Figure 5 represents the DOS plots for Pd-doped and Pd-decorated graphene before and after Hydrogen adsorption, resulting in both Pd-doped and Pd-decorated graphene enhancing electrical conductivity due to decreased HLG following the adsorption of the Hydrogen molecule.

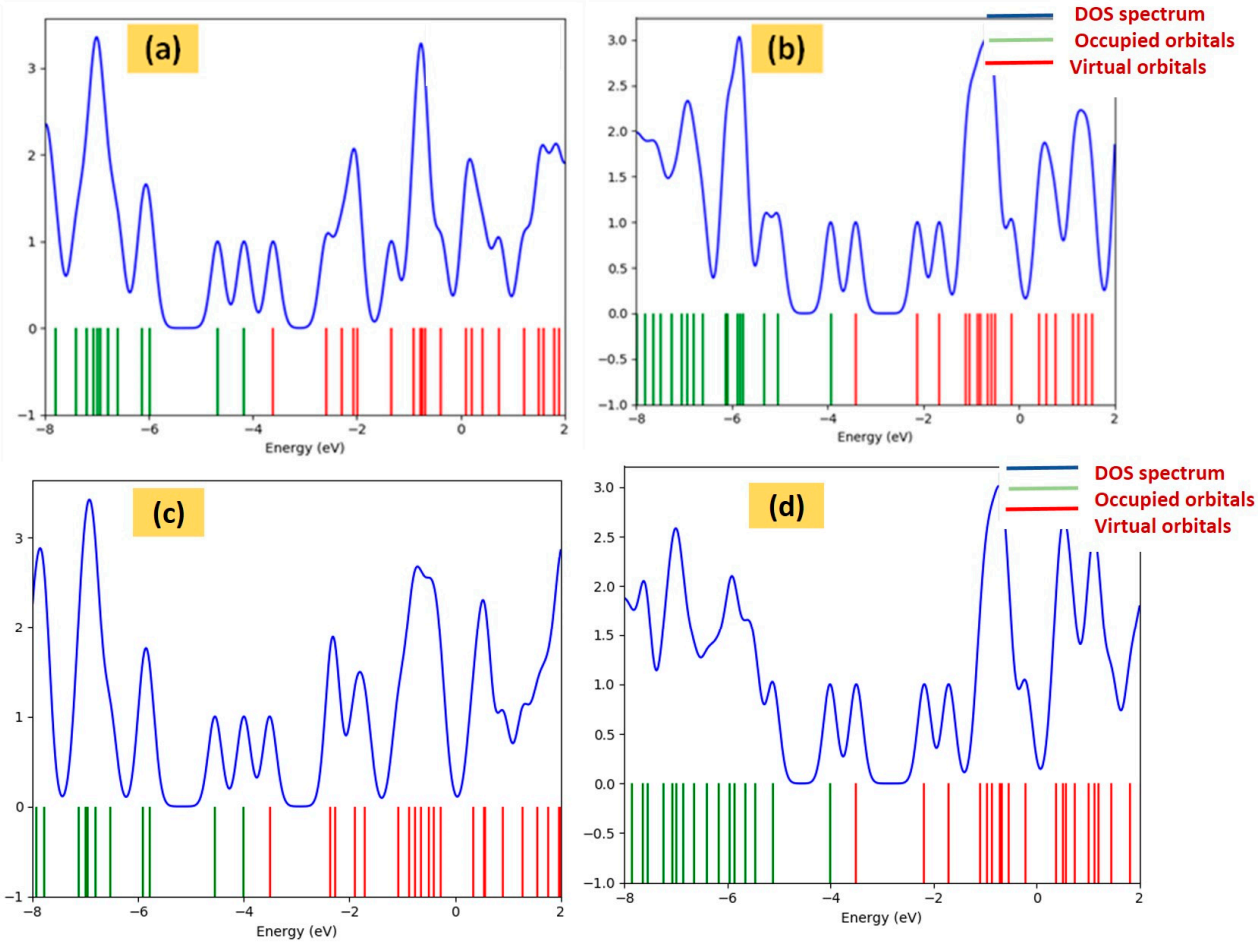


**Figure 5.** DOS plots shown in (**a**,**c**) for Pd doped graphene and (**b**,**d**) for Pd decorated graphene before and after adsorption of H2. Blue color indicates the DOS spectrum, green color indicates occupied orbitals and red color indicates virtual orbitals.

The Pd-decorated graphene shows a much lower HLG value in comparison to Pd-doped graphene given the changes in DOS plot gaps suggesting greater electrical conductivity for Pd-decorated graphene than Pd-doped graphene. The electrical conductivity depends on temperature and the value of HLG as shown in Equation (8) [62–64].

$$\sigma = AT^{3/2} \exp\left(\frac{-E_g}{2kT}\right) \quad (8)$$

As the value of HLG ($E_g$) increases, the value of electrical conductivity ($\sigma$) decreases due to the negative exponential in the expression and vice versa. In both Pd-doped and Pd-decorated graphene conditions, the value of HLG decreased. However, a comparison between Pd-doped and Pd-decorated graphene following hydrogen adsorption showed that the value of HLG decreased from 0.488 to 0.477 for Pd-doped and Pd-decorated graphene, respectively. Thus, as per Equation (8), electrical conductivity was higher for the Pd-decorated graphene. This shows that the Pd-decorated graphene is a better sensor for $H_2$ detection. Also, recovery time appears to play an essential role in the detection of gases and indicates the time consumption for the desorption of gases following adsorption. It is the desirable short recovery time for better gas sensor capabilities which can be obtained through the lowest value of the adsorption energy, as mentioned in the Equation (9) [62,65].

$$\tau = \upsilon_0^{-1} \exp\left(\frac{-E_{ads}}{kT}\right) \quad (9)$$

where $\tau$ stands for the recovery time, $E_{ads}$ for the adsorption energy, $\upsilon_0$ for the attempt frequency, T for temperature, and k for Boltzmann constant. As per the equation, the lower the value of adsorption energy, the lower the recovery time will be; this is one of the sensor's desirable attributes. As per the results, adsorption energy for the Pd-doped graphene was $-4.3$ eV and, for the Pd-decorated graphene, it was $-0.44$ eV. This is far lower than Pd-doped graphene, meaning that recovery time for the Pd-decorated graphene was much lower than Pd-decorated graphene. We can conclude, therefore, that Pd-decorated graphene is a better gas sensor than Pd-decorated graphene.

The distribution map for electron density with the projection of Pd-doped graphene and Pd-decorated graphene is shown in Figures 6a and 6b,c, respectively.

These maps showed that, for both Pd-doped graphene and Pd-decorated graphene, conditions electron density concentrated at the Pd atom. Pd-decorated graphene, however, showed a concentration of electron density at Pd (above the surface of graphene) when visualized using only 3D projection.

In addition to that, Figure 6d–f shows a projection map with the distribution of an electronic localisation function shown later [66–69] for both Pd-doped and Pd-decorated graphene. To determine the location of electron pairs, electron localisation function is a vital phenomenon [69]. As shown in the ELF graph, Figure 6d shows the location of electron pairs for Pd-doped conditions. It shows that, for Pd-doped graphene, electron pairs localised at the place where the Pd atom attached while, for Pd-decorated graphene, electron pairs are evenly distributed at the corner atoms, as depicted in Figure 6.

The condition for electron density contour plots, and electron localisation function plots with the projection of Pd-doped/decorated graphene after adsorption $H_2$ molecule, is shown in Figure 7.

Figure 7 shows that, for Pd-doped graphene after $H_2$ adsorption, the concentration of electron density shifted from the Pd atom to the $H_2$ molecule (Figure 7a,b), while there was no effect of electron density concentration over Pd-decorated graphene (Figure 7c,d). Because Pd atoms, unlike the doped condition, are not on the surface of the graphene in the decorated condition, the Pd atom localised at the surface of the graphene. Additionally, Figure 7e–h shows electron localisation function for Pd-doped/decorated graphene after $H_2$ adsorption. It shows that, following $H_2$ adsorption, the concentrated electron pairs in Pd-doped graphene are evenly distributed at the atom's corners. It also shows that, at

the point where the Pd atom was doped, no charge localisation occurred (Figure 7e,f). In contrast, for Pd-decorated graphene after $H_2$ adsorption, electron pairs were concentrated on the corner, at the location where $H_2$ was attached to a Pd atom (Figure 7g,h).

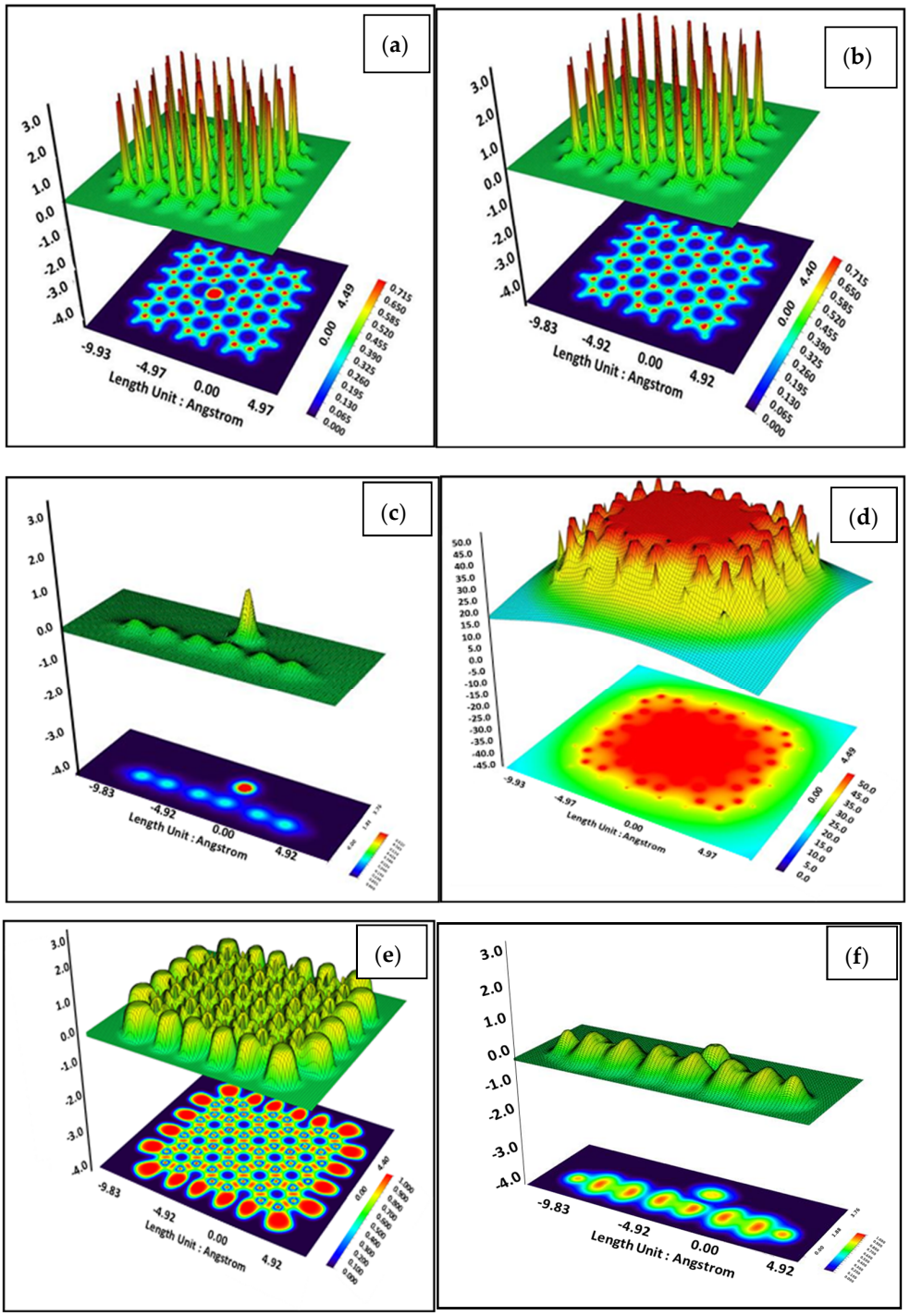


**Figure 6.** 2D and 3D Electron density contour plots of (**a**) Pd-doped graphene (**b**,**c**) Pd-decorated graphene and Electron localization function projections of (**d**) Pd-doped graphene (**e**,**f**) Pd-decorated graphene. The charge accumulation regions are in red, while the charge depletion regions are in blue.

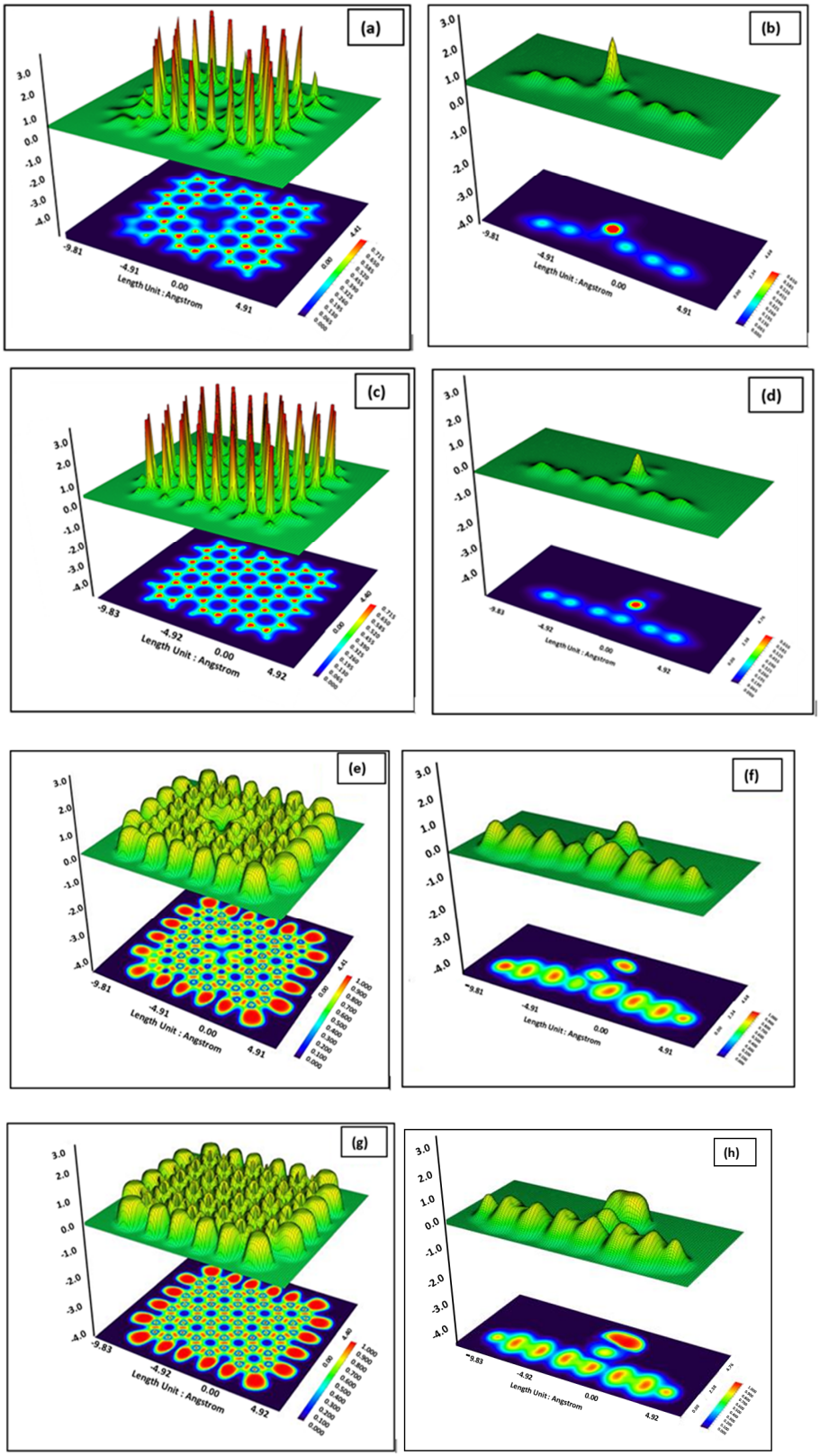


**Figure 7.** 2D and 3D Electron density contour plots and projections of: (**a**,**b**) Pd-doped graphene-$H_2$, (**c**,**d**) Pd-decorated graphene (G)-$H_2$, 2D and 3D Electron localization function plots, and projections of (**e**,**f**) Pd-decorated graphene (G)-$H_2$ and (**g**,**h**) Pd-decorated graphene-$H_2$. The charge accumulation regions are in red, while the charge depletion regions are in blue.

## 4. Conclusions

In the present work, the sensing capabilities of Pd-doped graphene and Pd-decorated graphene were investigated through DFT calculations of hydrogen molecules. Properties of these clusters were analysed by using the value of bond distance, adsorption energy, and NBO population analysis. During the adsorption of the $H_2$ molecule, charge transfer from the $H_2$ molecule to the Pd-doped and Pd-decorated graphene clusters occurred. This shows that Pd-doped/decorated graphene behaves as an electron acceptor. Further results show that decreases to the HLG values of Pd-doped and Pd-decorated graphene increases the electrical conductivity for both Pd-doped and Pd-decorated graphene following adsorption of $H_2$. While analysing a comparison between Pd-doped and Pd-decorated graphene for the adsorption of $H_2$ molecule, the chemical activity and electrical conductivity are higher for Pd-decorated graphene in comparison to Pd-doped graphene. In contrast, the charge transfer of Pd-doped graphene is better than Pd-decorated graphene. Furthermore, recovery time is much lower for Pd-decorated graphene compared to Pd-doped graphene. It can be concluded, therefore, that the Pd-decorated graphene has much better sensing capabilities compared to Pd-doped graphene and, therefore, the analysed sensing film can be envisioned as a potential nanosensor platform.

**Author Contributions:** Conceptualization, A.G. and A.Y.; resources, A.G. and A.Y.; writing—original draft preparation, V.K. and A.Y.; writing—review and editing, V.K., A.Y.; supervision and project administration, K.M. and A.G. All authors have read and agreed to the published version of the manuscript.

**Funding:** This research received no external funding.

**Acknowledgments:** Authors gratefully acknowledge Start Research Grant (SRG/2020/001895) provided by Science and Engineering Research Board, Department of Science and Technology, India. Kunal Mondal gratefully acknowledges the Energy & Environment S & T at the Idaho National Laboratory, the USA for their support.

**Conflicts of Interest:** The authors declare no conflict of interest. The funders had no role in the design of the study; in the collection, analyses, or interpretation of data; in the writing of the manuscript, or in the decision to publish the results.

## References

1. Ji, H.; Zeng, W.; Li, Y. Gas sensing mechanisms of metal oxide semiconductors: A focus review. *Nanoscale* **2019**, *11*, 22664–22684. [CrossRef] [PubMed]
2. Gupta, A.; Pandey, S.S.; Nayak, M.; Maity, A.; Majumder, S.B.; Bhattacharya, S. Hydrogen sensing based on nanoporous silica-embedded ultra dense ZnO nanobundles. *RSC Adv.* **2014**, *4*, 7476–7482. [CrossRef]
3. Kaskhedikar, N.A.; Maier, J. Lithium Storage in carbon nanostructures. *Adv. Mater.* **2009**, *21*, 2664–2680. [CrossRef]
4. Zhu, Y.; Murali, S.; Cai, W.; Li, X.; Suk, J.W.; Potts, J.R.; Ruoff, R.S. Graphene and graphene oxide: Synthesis, properties, and applications. *Adv. Mater.* **2010**, *22*, 3906–3924. [CrossRef]
5. Wang, Y.; Li, Z.; Wang, J.; Li, J.; Lin, Y. Graphene and graphene oxide: Biofunctionalization and applications in biotechnology. *Trends Biotechnol.* **2011**, *29*, 205–212. [CrossRef]
6. Esrafili, M.D.; Dinparast, L. The selective adsorption of formaldehyde and methanol over Al- or Si-decorated graphene oxide: A DFT study. *J. Mol. Graph. Model.* **2018**, *80*, 25–31. [CrossRef] [PubMed]
7. Novoselov, K.S.; Geim, A.K.; Morozov, S.V.; Jiang, D.; Zhang, Y.; Dubonos, S.V.; Grigorieva, I.V.; Firsov, A.A. Electric field in atomically thin carbon films. *Science* **2004**, *306*, 666–669. [CrossRef]
8. Li, X.; Wang, X.; Zhang, L.; Lee, S.; Dai, H. Chemically derived, ultrasmooth graphene nanoribbon semiconductors. *Science* **2008**, *319*, 1229–1232. [CrossRef]
9. Neto, A.H.C.; Guinea, F.; Peres, N.M.R.; Novoselov, K.; Geim, A.K. The electronic properties of graphene. *Rev. Mod. Phys.* **2009**, *81*, 109–162. [CrossRef]
10. Lahiri, J.; Lin, Y.; Bozkurt, P.; Oleynik, I.; Batzill, M. An extended defect in graphene as a metallic wire. *Nat. Nanotechnol.* **2010**, *5*, 326–329. [CrossRef]
11. Choi, H.J.; Jung, S.-M.; Seo, J.-M.; Chang, D.W.; Dai, L.; Baek, J.-B. Graphene for energy conversion and storage in fuel cells and supercapacitors. *Nano Energy* **2012**, *1*, 534–551. [CrossRef]
12. Bonaccorso, F.; Colombo, L.; Yu, G.; Stoller, M.; Tozzini, V.; Ferrari, A.C.; Ruoff, R.S.; Pellegrini, V. Graphene, related two-dimensional crystals, and hybrid systems for energy conversion and storage. *Science* **2015**, *347*, 1246501. [CrossRef] [PubMed]
13. Kamat, P.V. Graphene-based nanoassemblies for energy conversion. *J. Phys. Chem. Lett.* **2011**, *2*, 242–251. [CrossRef]

14. Yoon, H.J.; Jun, D.H.; Yang, J.H.; Zhou, Z.; Yang, S.S.; Cheng, M.M.-C. Carbon dioxide gas sensor using a graphene sheet. *Sens. Actuators B Chem.* **2011**, *157*, 310–313. [CrossRef]
15. Zhang, B.; Cui, T. An ultrasensitive and low-cost graphene sensor based on layer-by-layer nano self-assembly. *Appl. Phys. Lett.* **2011**, *98*, 073116. [CrossRef]
16. Rad, A.S. Density functional theory study of the adsorption of MeOH and EtOH on the surface of Pt-decorated graphene. *Phys. E Low-Dimens. Syst. Nanostruct.* **2016**, *83*, 135–140. [CrossRef]
17. Hughes, Z.E.; Walsh, T.R. Computational chemistry for graphene-based energy applications: Progress and challenges. *Nanoscale* **2015**, *7*, 6883–6908. [CrossRef] [PubMed]
18. Perreault, F.; Faria, A.F.; Elimelech, M. Environmental applications of graphene-based nanomaterials. *Chem. Soc. Rev.* **2015**, *44*, 5861–5896. [CrossRef] [PubMed]
19. Prezhdo, O.V.; Kamat, P.V.; Schatz, G.C. Virtual issue: Graphene and functionalized graphene. *J. Phys. Chem. C* **2011**, *115*, 3195–3197. [CrossRef]
20. Wanno, B.; Tabtimsai, C. A DFT investigation of CO adsorption on VIIIB transition metal-doped graphene sheets. *Superlattices Microstruct.* **2014**, *67*, 110–117. [CrossRef]
21. Sun, Y.; Chen, L.; Zhang, F.; Li, D.; Pan, H.; Ye, J. First-principles studies of HF molecule adsorption on intrinsic graphene and Al-doped graphene. *Solid State Commun.* **2010**, *150*, 1906–1910. [CrossRef]
22. Ri, N.-C.; Wi, J.-H.; Kim, N.-H.; Ri, S.-I. First principles study on the structural, electronic, and transport properties of the Armchair Graphane, fluorographene, fluorographane/graphene heterostructure nanoribbons terminated by H and F atoms. *Phys. E Low-Dimens. Syst. Nanostruct.* **2019**, *108*, 226–232. [CrossRef]
23. Song, E.H.; Wen, Z.; Jiang, Q. CO Catalytic oxidation on copper-embedded graphene. *J. Phys. Chem. C* **2011**, *115*, 3678–3683. [CrossRef]
24. Zhang, T.; Xue, Q.; Shan, M.; Jiao, Z.; Zhou, X.; Ling, C.; Yan, Z. Adsorption and catalytic activation of $O_2$ molecule on the surface of Au-doped graphene under an external electric field. *J. Phys. Chem. C* **2012**, *116*, 19918–19924. [CrossRef]
25. Ma, L.; Zhang, J.-M.; Xu, K.-W.; Ji, V. A first-principles study on gas sensing properties of graphene and Pd-doped graphene. *Appl. Surf. Sci.* **2015**, *343*, 121–127. [CrossRef]
26. Li, Y.; Zhou, Z.; Yu, G.; Chen, W.; Chen, Z. CO catalytic oxidation on iron-embedded graphene: Computational quest for low-cost nanocatalysts. *J. Phys. Chem. C* **2010**, *114*, 6250–6254. [CrossRef]
27. Huang, C.; Ye, X.; Chen, C.; Lin, S.; Xie, D. A computational investigation of CO oxidation on ruthenium-embedded hexagonal boron nitride nanosheet. *Comput. Theor. Chem.* **2013**, *1011*, 5–10. [CrossRef]
28. Wu, M.; Cao, C.; Jiang, J.Z. Electronic structure of substitutionally Mn-doped graphene. *New J. Phys.* **2010**, *12*, 063020. [CrossRef]
29. Gupta, A.; Gangopadhyay, S.; Gangopadhyay, K.; Bhattacharya, S. Palladium-functionalized nanostructured platforms for enhanced hydrogen sensing. *Nanomater. Nanotechnol.* **2016**, *6*, 40. [CrossRef]
30. Gupta, A.; Srivastava, A.; Mathai, C.J.; Gangopadhyay, K.; Gangopadhyay, S.; Bhattacharya, S. Nano porous palladium sensor for sensitive and rapid detection of hydrogen. *Sens. Lett.* **2014**, *12*, 1279–1285. [CrossRef]
31. Gupta, A.; Parida, P.K.; Pal, P. *Functional Films for Gas Sensing Applications: A Review*; Springer: Singapore, 2019.
32. Alfano, B.; Polichetti, T.; Miglietta, M.L.; Massera, E.; Schiattarella, C.; Ricciardella, F.; Di Francia, G. Fully eco-friendly H 2 sensing device based on Pd-decorated graphene. *Sens. Actuators B Chem.* **2017**, *239*, 1144–1152. [CrossRef]
33. Singla, M.; Jaggi, N. Enhanced hydrogen sensing properties in copper decorated nitrogen doped defective graphene nanoribbons: DFT study. *Phys. E Low-Dimens. Syst. Nanostruct.* **2021**, *131*, 114756. [CrossRef]
34. Bakhshi, F.; Farhadian, N. Co-doped graphene sheets as a novel adsorbent for hydrogen storage: DFT and DFT-D3 correction dispersion study. *Int. J. Hydrogen Energy* **2018**, *43*, 8355–8364. [CrossRef]
35. Zhou, Q.; Yong, Y.; Ju, W.; Su, X.; Li, X.; Wang, C.; Fu, Z. DFT study of the adsorption of 2, 3, 7, 8-tetrachlorodibenzofuran (TCDF) on vacancy-defected graphene doped with Mn and Fe. *Curr. Appl. Phys.* **2018**, *18*, 61–67. [CrossRef]
36. Orazi, V.; Ambrusi, R.; Marchetti, J.; Pronsato, M. DFT study of the hydrogen adsorption and storage on $Ni_4$ cluster embedded in multivacancy graphene. *Int. J. Hydrogen Energy* **2020**, *45*, 30805–30817. [CrossRef]
37. Tian, W.; Zhang, Y.; Wang, Y.; Liu, T.; Cui, H. A study on the hydrogen storage performance of graphene–Pd(T)–graphene structure. *Int. J. Hydrogen Energy* **2020**, *45*, 12376–12383. [CrossRef]
38. Gecim, G.; Ozekmekci, M.; Fellah, M. Ga and Ge-doped graphene structures: A DFT study of sensor applications for methanol. *Comput. Theor. Chem.* **2020**, *1180*, 112828. [CrossRef]
39. Zheng, N.; Yang, S.; Xu, H.; Lan, Z.; Wang, Z.; Gu, H. A DFT study of the enhanced hydrogen storage performance of the Li-decorated graphene nanoribbons. *Vacuum* **2020**, *171*, 109011. [CrossRef]
40. Ostad, F.Z.; Ghazi, M.; Javan, M.; Izadifard, M. DFT study of Ptn, Pdn, and Irn ($n$ = 5, 6) clusters adsorbed on graphene: Structural and electronic properties. *Phys. B Condens. Matter* **2019**, *575*, 411678. [CrossRef]
41. Montejo-Alvaro, F.; Rojas-Chávez, H.; Román-Doval, R.; Mtz-Enriquez, A.; Cruz-Martínez, H.; Medina, D. Stability of Pd clusters supported on pristine, B-doped, and defective graphene quantum dots, and their reactivity toward oxygen adsorption: A DFT analysis. *Solid State Sci.* **2019**, *93*, 55–61. [CrossRef]
42. Amaya-Roncancio, S.; Blanco, A.G.; Linares, D.; Sapag, K. DFT study of hydrogen adsorption on Ni/graphene. *Appl. Surf. Sci.* **2018**, *447*, 254–260. [CrossRef]

43. Cui, H.; Zhang, X.; Chen, D.; Tang, J. Pt & Pd decorated CNT as a workable media for SOF2 sensing: A DFT study. *Appl. Surf. Sci.* **2018**, *471*, 335–341. [CrossRef]
44. Cheng, J.; Hu, D.; Yao, A.; Gao, Y.; Asadi, H. A computational study on the Pd-decorated ZnO nanocluster for H2 gas sensing: A comparison with experimental results. *Phys. E Low-Dimens. Syst. Nanostruct.* **2020**, *124*, 114237. [CrossRef]
45. Khodadadi, Z. Evaluation of H2S sensing characteristics of metals–doped graphene and metals-decorated graphene: Insights from DFT study. *Phys. E Low-Dimens. Syst. Nanostruct.* **2018**, *99*, 261–268. [CrossRef]
46. Kohn, W.; Sham, L. Self-consistent equations including exchange and correlation effects. *Phys. Rev.* **1965**, *140*, A1133. [CrossRef]
47. Frisch, M.J.; Trucks, G.W.; Schlegel, H.B.; Scuseria, G.E.; Robb, M.A.; Cheeseman, J.R.; Scalmani, G.; Barone, V.; Petersson, G.A.; Nakatsuji, H.; et al. *Gaussian 09, Revision d. 01*; Gaussian Inc.: Wallingford, CT, USA, 2009.
48. O'Boyle, N.M.; Tenderholt, A.L.; Langner, K. cclib: A library for package-independent computational chemistry algorithms. *J. Comput. Chem.* **2008**, *29*, 839–845. [CrossRef]
49. Foresman, J.B. *Exploring Chemistry with Electronic Structure Methods: A Guide to Using Gaussian*, 2nd ed.; Gaussian Inc.: Pittsburgh, PA, USA, 1996.
50. Kulkarni, B.S.; Krishnamurty, S.; Pal, S. Probing Lewis acidity and reactivity of Sn- and Ti-beta zeolite using industrially important moieties: A periodic density functional study. *J. Mol. Catal. A Chem.* **2010**, *329*, 36–43. [CrossRef]
51. Modi, C.K.; Trivedi, P.M.; Chudasama, J.A.; Nakum, H.D.; Parmar, D.K.; Gupta, S.; Jha, P.K. Zeolite-Y entrapped bivalent transition metal complexes as hybrid nanocatalysts: Density functional theory investigation and catalytic aspects. *Green Chem. Lett. Rev.* **2014**, *7*, 278–287. [CrossRef]
52. Geerlings, P.; De Proft, A.F.; Langenaeker, W. Conceptual density functional theory. *Chem. Rev.* **2003**, *103*, 1793–1874. [CrossRef]
53. Parr, R.G.; Szentpály, L.V.; Liu, S. Electrophilicity index. *J. Am. Chem. Soc.* **1999**, *121*, 1922–1924. [CrossRef]
54. Janak, J.F. Proof that$\partial E/\partial n_i = \varepsilon$ in density-functional theory. *Phys. Rev. B* **1978**, *18*, 7165–7168. [CrossRef]
55. Pearson, R.G. Chemical hardness and density functional theory. *J. Chem. Sci.* **2005**, *117*, 369–377. [CrossRef]
56. Pearson, R.G. The electronic chemical potential and chemical hardness. *J. Mol. Struct. TheoChem.* **1992**, *255*, 261–270. [CrossRef]
57. Nobel, N.; Bamba, K.; Patrice, O.; Ziao, N. NBO population analysis and electronic calculation of four azopyridine ruthenium complexes by DFT method. *Comput. Chem.* **2017**, *5*, 51–64. [CrossRef]
58. Pan, S.; Solà, M.; Chattaraj, P.K. On the validity of the maximum hardness principle and the minimum electrophilicity principle during chemical reactions. *J. Phys. Chem. A* **2013**, *117*, 1843–1852. [CrossRef] [PubMed]
59. Pearson, R.G. The principle of maximum hardness. *Accounts Chem. Res.* **1993**, *26*, 250–255. [CrossRef]
60. Mao, S.; Zhou, H.; Wu, S.; Yang, J.; Li, Z.; Wei, X.; Wang, X.; Wang, Z.; Li, J. High performance hydrogen sensor based on Pd/$TiO_2$ composite film. *Int. J. Hydrogen Energy* **2018**, *43*, 22727–22732. [CrossRef]
61. Raghu, S.; Ramaprabhu, S. Nanostructured palladium modified graphitic carbon nitride–High performance room temperature hydrogen sensor. *Int. J. Hydrogen Energy* **2016**, *41*, 20779–20786. [CrossRef]
62. Hadipour, N.L.; Peyghan, A.A.; Soleymanabadi, H. Theoretical study on the Al-doped ZnO nanoclusters for CO chemical sensors. *J. Phys. Chem. C* **2015**, *119*, 6398–6404. [CrossRef]
63. Yong, Y.; Jiang, H.; Lv, S.; Cao, J.; Li, X. The cluster-assembled nanowires based on M12N12 (M = Al and Ga) clusters as potential gas sensors for CO, NO, and $NO_2$ detection. *Phys. Chem. Chem. Phys.* **2016**, *18*, 21431–21441. [CrossRef] [PubMed]
64. Bhuvaneswari, R.; Nagarajan, V.; Chandiramouli, R. First-principles insights on the electronic and field emission properties of Ga and Al doped germanium nanocones. *J. Electron Spectrosc. Relat. Phenom.* **2018**, *227*, 15–22. [CrossRef]
65. Beheshtian, J.; Peyghan, A.A.; Bagheri, Z. Detection of phosgene by Sc-doped BN nanotubes: A DFT study. *Sens. Actuators B Chem.* **2012**, *171–172*, 846–852. [CrossRef]
66. Savin, A.; Becke, A.D.; Flad, J.; Nesper, R.; Preuss, H.; Von Schnering, H.G. A new look at electron localization. *Angew. Chem. Int. Ed.* **1991**, *30*, 409–412. [CrossRef]
67. Becke, A.D.; Edgecombe, E.K. A simple measure of electron localization in atomic and molecular systems. *J. Chem. Phys.* **1990**, *92*, 5397–5403. [CrossRef]
68. Silvi, B.; Savin, A. Classification of chemical bonds based on topological analysis of electron localization functions. *Nature* **1994**, *371*, 683–686. [CrossRef]
69. Fuentealba, P.; Chamorro, E.; Santos, J.C. Chapter 5 Understanding and using the electron localization function. In *Theoretical Aspects of Chemical Reactivity*; 2007; Elsevier: Amsterdam, The Netherlands; Volume 19, pp. 57–85. [CrossRef]